IEEE Access
Multidisciplinary | Rapid Review | Open Access Journal

SPECIAL SECTION ON COLLABORATION FOR INTERNET OF THINGS

Received July 7, 2018, accepted August 5, 2018, date of publication August 13, 2018, date of current version September 21, 2018.

Digital Object Identifier 10.1109/ACCESS.2018.2865209

Separation of Vehicle Detection Area Using Fourier Descriptor Under Internet of Things Monitoring

HONGHUI FAN[1] AND HONGJIN ZHU[1, 2]

[1]School of Computer Engineering, Jiangsu University of Technology, Changzhou 213001, China
[2]Key Laboratory of Cloud Computing and Intelligent Information Processing of Changzhou City, Jiangsu University of Technology, Changzhou 213001, China

Corresponding author: Honghui Fan (fanhonghui@jsut.edu.cn)

This work was supported in part by the Natural Science Fund of Changzhou under Grant CE20165028 and Grant CE20175026, in part by the Qing Lan Project of Jiangsu Province, and in part by the Natural Science Research Project of Jiangsu Province under Grant BY2016030-05.

ABSTRACT With the popularity of automobiles, road traffic accidents and congestion have become increasingly serious. Therefore, technologies are needed to solve problems such as speeding and congestion. The detection and tracking of vehicles based on computer vision and Internet of Things monitoring are an important part of the intelligent traffic monitoring system. The angle between the camera and the vehicle will cause the gradually moving vehicles to have a connection during image segmentation. This paper aims to improve the detection accuracy of vehicles from camera images. A new separation method of the vehicle detection area was proposed in this paper. Moving areas are extracted by inter-frame differences, and vehicle areas are formed from the areas. If more than one vehicle area partially overlaps as one area, it is necessary to separate the area. The existing method extracts a place to be separated from an outline of the area. However, it is impossible for the method to separate vehicles using the extracted shape. Therefore, a new method is proposed that makes the place to be separated defined by the reshaping of the area with the use of the Fourier descriptor. The method tries to detect the place from the area. As a result, this method makes it possible to separate the area that the existing method cannot separate and it has obtained a high accuracy of separation in the experimental data of the Internet of Things monitoring.

INDEX TERMS Internet of Things monitoring, vehicle area detection, overlap segmentation, Fourier descriptor, Hough transformation, precise segmentation.

I. INTRODUCTION

With the increase in vehicles running on the road, some problems such as accidents and traffic congestion on the road are increasing [1]. Therefore, an intelligent transportation system the Internet of Things is necessary, which could solve traffic problems like congestion, speeding, and traffic flow [2], [3]. A wireless device is used to detect vehicles' speeds, and this method is widely used in vehicle information acquisition systems on the road [4]. However, that method has a problem since it is hard to detect multiple vehicles concurrently over a large range [5].

In recent years, pattern recognition methods and Internet of Things technologies have been widely used to detect speed based on traffic surveillance video [6], [7]. Based on the video surveillance method, it is not necessary to pay attention to the camera installations [8], and it can also detect multiple vehicles concurrently over a large range [9]. Currently, the intelligent transportation system based on computer vision and Internet of Things mainly extracts the target from the captured image in order to form and track the vehicle area [10]. In addition, it could analyze various types of vehicle data and could provide information besides velocity detection [11]. However, separating the partially overlapping vehicle areas into separate areas is not perfect when forming a vehicle area [12], [13]. Therefore, this paper would pay attention to vehicle detection using Internet of Things traffic surveillance video with a camera mounted on the road. The impact of the environment, the installation angle of equipment and other factors may cause vehicle visual occlusion in traffic videos, and the occlusion could result in the error of vehicle detection and tracking [14]. Some researchers have focused on researching vehicle detection

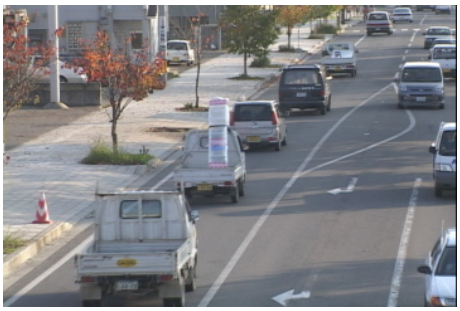

(a)

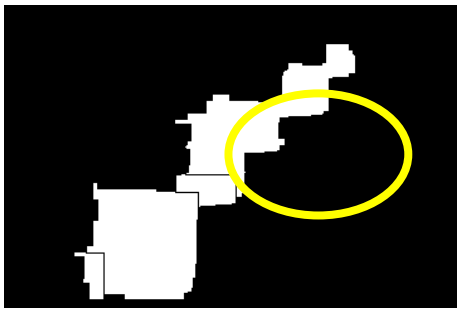

(b)

FIGURE 1. Overlap problem in the vehicle area detection process. (a) Original image. (b) Vehicle area detection.

and tracking and proposed many methods to improve detection accuracy [15], [16]. Many research results showed that the moving objects had been extracted from the captured images [17], [18] and that the vehicle area formation and tracking had been successful [19], [20]. When two or more vehicles partially overlap in the original image, the plurality of vehicle areas was regarded as one vehicle area [21]. Therefore, there was a problem with inaccurate separation when the vehicle area was formed [22], and it was not very good at separating partially overlapping vehicle areas into separate areas [23], [24]. The entire vehicle area is formed by the outline image of the vehicle obtained from the difference image [23], [25]. For this purpose, the area of the vehicle is marked after expansion by the expansion process, and then the extraction area was reduced by the erosion process [26], [27]. Since unnecessary regions such as vehicle shadows were also extracted, the removal of unnecessary vehicle regions is also researched [28], [29].

In this research, we focus on processing such a separation of overlapping vehicles. In order to improve the accuracy of vehicle extraction and the number of vehicles from Internet of Things traffic surveillance video, a new vehicle area separation method based on the Fourier Descriptor was proposed.

II. VEHICLE AREA SEPARATION

A. VEHICLE CONNECTION PROBLEM ON INTERNET OF THINGS SURVEILLANCE VIDEO

According to the position and angle of the Internet of Things surveillance monitoring equipment, it often happens that vehicles overlap each other, as shown in Figure 1(a).

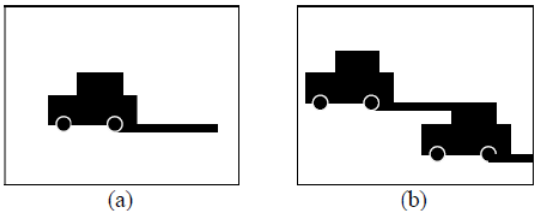

(a) (b)

FIGURE 2. Vehicle shadows cause vehicle detection overlap.

Figure 1(b) is the result of the vehicle area being extracted based on the background difference method from the original image. From the experimental results, it was proved that a plurality of vehicle regions was considered as one vehicle region based on the background difference, which would result in greater errors in vehicle detection. If the vehicle area separation failed, the vehicle tracking would not succeed before the focused frame t. Therefore, it was necessary to address area separation when multiple vehicle areas overlap each other.

The connected pixels in the collective areas of frame t and frame $t-1$ were used when tracking object vehicles. Therefore, if multiple vehicle areas in frame t could not be separated smoothly and extracted as separate areas, only the vehicle areas that had the most connected pixels in the collective areas of frame t and frame $t+1$ could be tracked, even if multiple vehicle areas in frame $t+1$ were separated correctly.

Although an inter-frame difference can be used to extract a running vehicle, the area extracted in Figure 2(a) contains a shaded area. By including the shadow area, the vehicle's shadow and other vehicles are connected, as shown in Figure 2(b). As a result, when the vehicles are connected to each other, a plurality of vehicles becomes one area. Therefore, the shadow area is deleted by using the color information to designate the pixels as the shadow area.

Since the value that is input to the display and the value actually displayed on the display are different in their *RGB* colors, gamma correction is performed. γ is a gamma value that varies depending on the device and computer system, and it was set to 2 in this research. $L*a*b*$ color model can preserve as wide gamut and rich color as possible in image processing.

$$\begin{bmatrix} X \\ Y \\ Z \end{bmatrix} = \begin{bmatrix} 40.9568 & 35.5041 & 17.9167 \\ 21.3389 & 70.6743 & 7.98680 \\ 1.86297 & 11.4620 & 91.2367 \end{bmatrix} \begin{bmatrix} \left(\frac{R}{255}\right)^{\gamma} \\ \left(\frac{G}{255}\right)^{\gamma} \\ \left(\frac{B}{255}\right)^{\gamma} \end{bmatrix} \tag{1}$$

In order to represent the color information of vehicle shadow more effectively, *RGB* color model is converted to $L*a*b*$ color model. Therefore, converting *RGB* to *XYZ* colors is expressed as Formula (1).

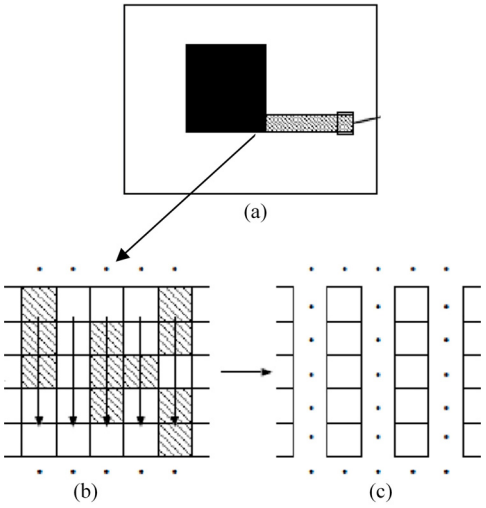

FIGURE 3. Vehicle shadow area elimination diagram. (a) Horizontal extension of the shadow. (b) The enlargement of the Extended shadow. (c) Elimination of extended shadow.

Next, using the obtained XYZ, the conversion from Formula (2) to (4) of $L*a*b*$ is performed.

$$L^* = \begin{cases} 116\left(\frac{Y}{Y_n}\right)^{\frac{1}{3}} - 16 \left(while \frac{Y}{Y_n} > 0.008856\right) \\ 903.29\left(\frac{Y}{Y_n}\right) other \end{cases} \quad (2)$$

$$a^* = 500\left\{\left(\frac{X}{X_n}\right)^{\frac{1}{3}} - \left(\frac{Y}{Y_n}\right)^{\frac{1}{3}}\right\} \quad (3)$$

$$b^* = 200\left\{\left(\frac{Y}{Y_n}\right)^{\frac{1}{3}} - \left(\frac{Z}{Z_n}\right)^{\frac{1}{3}}\right\} \quad (4)$$

The range of possible values for the shaded $a*b*$ is defined in Formula (5). The reason why the value of $L*$ is not shown is that it varies greatly depending on the time zone. Therefore, it is only necessary to read the color information of the area for each time and update the $L*$ value at any time. The pixels satisfying all of the $L*$ values, $a*$ values and $b*$ values shown in Formula (5) are determined as the pixels of the hatched area. The image information of the vehicle shadow in different time periods was investigated and analyzed. The results show that the value of the luminance L is different in different time periods, but the distribution of a and b is stable, therefore, we get the range of the value of a and b according to the analysis results of multiple vehicle shadow images.

$$\begin{aligned} -3.0 < a* < 2.0 \\ -10.0 < b* < 2.0 \end{aligned} \quad (5)$$

Figure 3(a) shows the horizontally extending shadow. The black part is the vehicle, and the gray part is the shaded area. Figure 3(b) is an enlarged view of the shaded area of Figure 3(a). The shaded portion is the pixel that is determined by the $L*a*b*$ value as a shaded area. Here, in order to delete the shadow area, the pixel of the target area is set to 1 and the background pixel is set to 0. As shown in Figure 3(b), the total number of pixels n is checked for the pixel columns with pixel values of 1 as presented downward from the pixels (x, y) of $i(x, y) = 1$ and $i(x, y-1) = 0$. At the same time, the number of pixels s determined by the $L*a*b*$ value as a hatched area is checked downward from (x, y). Using these values, we delete the shadow based on Formula (6).

$$Column\ of\ connected\ pixels = \begin{cases} 1 : \frac{n}{2} \le s \\ 0 : \frac{n}{2} > s \end{cases} \quad (6)$$

When the number of pixels s determined to be shaded by the $L*a*b*$ value is equal to or greater than half of the total number of pixels n, the shading is deleted in the vertical direction. The front glass part of the vehicle may be removed, if eliminate the pixels of the vehicle shadow directly, so the number of pixels in each column is compared with the number of pixels in the detected vehicle shadow, the Figure 3(b) is processed according to the Formula (6), and the result is shown in Figure 3(c).

B. VEHICLE EDGE EXTRACTION

The vehicle's edge is a boundary with a large change in its density value at the boundary between adjacent areas. The Laplacian operator was used to extract the edge of the filter in our research. It was a second derivative, and it could detect object contours.

The vehicle's edge was a boundary with a large change in the density values at the boundary between each area. In our research, the Laplacian operator was used to extract the edge of the filter. The Laplacian was a second derivative and detects contours [30], [31], it can be shown that the simplest isotropic derivative operator is the Laplacian. After comparing the characteristics of various differential operators, Laplacian operator is used. The object pixel was denoted by $f(x, y)$, and then the 8-field second-order derivative $L(x, y)$ of $f(x, y)$ could be calculated. The second-order differential $L(x, y)$ was expressed as follows:

$$\begin{aligned} L(x, y) = & f(x-1, y-1) + f(x, y-1) \\ & + f(x+1, y-1) + f(x-1, y) \\ & + f(x+1, y) + f(x-1, y+1) \\ & + f(x, y+1) + f(x+1, y+1) - 8f(x, y) \end{aligned} \quad (7)$$

Let $I(x, y)$ be the brightness value of the coordinate (x, y), and find $L(x, y)$ using Formula (7). In order to obtain the value of $L(x, y)$ from 0 to 255, a linear conversion is performed. Assuming that the maximum value of L in the pixels in the image is L_{max} and the minimum value thereof is L_{min}, the linear transformation $g(x, y)$ is represented as follows:

$$g(x, y) = 255 \times \frac{L(x, y) - L_{min}}{L_{max} - L_{min}} \quad (8)$$

Threshold processing is performed on the $g(x, y)$ obtained by the linear transformation. A value equal to or greater

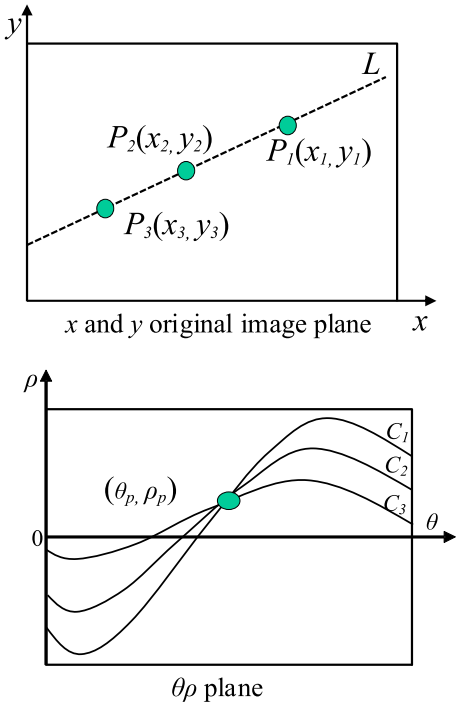

FIGURE 4. $\theta\rho$-Hough transformation based on the (x, y) original image plane and the θp plane.

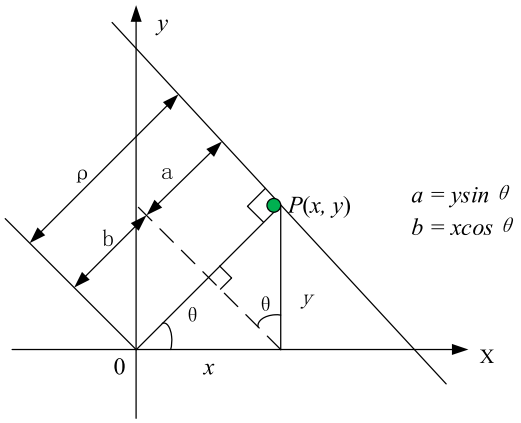

FIGURE 5. $\theta\rho$. The geometric relationship between point (x, y), θ and ρ.

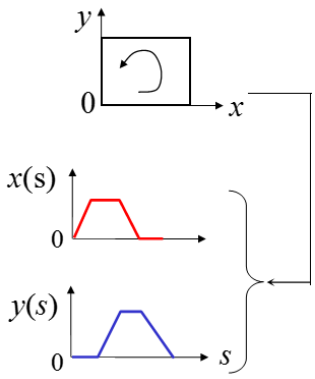

FIGURE 6. Synoptic diagram of the *G*-type Fourier descriptor.

than the threshold is replaced with a pixel value of 1, and otherwise, it is replaced with a pixel value of 0 to make it a binary image.

When the vehicle area was separated by the conventional chain code, the area may not be separated depending on the shape of the vehicle area obtained by the difference. In order to better separate the fields of vehicles, first a straight line was extracted, which pointed in the direction where the moving vehicles were headed. Next, the straight line and the affine transform were used to pivot and transform the vehicle area. In addition, Fourier descriptors were applied to the vehicle area and histograms were also used in order to make it easier to distinguish vehicle overlap areas. The Hough transform, as a method of extracting a straight line, can extract the straight line from an edge picture, which was transformed into a pixel. Based on applying the Hough transform, multiple lines were extracted from the edge image.

The $\theta\rho$-Hough transform extracted the most basic and highly available straight line. As shown in Figure 4, when the image was scanned to detect the figure pixel $P_1(x_1, y_1)$, the coordinate (x_1, y_1) was substituted into x and y in the expression as follows:

$$\rho = x\cos\theta + y\sin\theta \tag{9}$$

θ is the angle of the vertical line when the line connecting the origin and point (x, y) is perpendicular to the line passing through the point (x, y). ρ is the distance from the origin to the point (x, y). Substituting the coordinates (θ_p, ρ_p) in Figure 2 into Formula (9) yields a linear equation expressed as a straight line passing through three points in the original image. By performing this processing on the graphical pixels in the image, straight lines can be extracted from the original image.

On the basis of the relation of θ and ρ from Formula (9), it was available to express the curve C_1 on the θp curved surface by using the relational expression of θ_p and ρ. In the same way, then, curves C_2 and C_3 were obtained by using the coordinates (x_2, y_2) and (x_3, y_3) as well.

As shown in Figure. 4(a), the pattern pixels P_1, P_2, and P_3 are on the straight line L. At this point, curves C_1, C_2, and C_3 intersect at one point (θ_p, ρ_p) in Figure 2(b). This corresponds to the fact that there is only one common straight line L through the three points P_1, P_2, and P_3. The reason for this result is that θ and ρ in Formula (9) represent θ and ρ in Figure 5.

III. VEHICLE AREA SEPARATION USING FOURIER DESCRIPTOR

The *G* Fourier descriptor was proposed by *G. H.* Grunlund, and, as shown in Figure 6, the descriptor can only be used for closed curves, which means that it can be used to separate vehicles [32]. Considering the curve on the curved surface (x, y), if the position coordinates (x, y) of this curve were expressed by a complex curved surface, it can be expressed as follows:

$$z(s) = x(s) + jy(s) \tag{10}$$

The j in Formula (3) is $j = \sqrt{-1}$, and it is an imaginary unit. s is the real number over 0. Considering the closed curve counterclockwise from the origin, $z(s)$ is a periodic function in which the start point and the end point coincide with the closed curve and no discontinuous point occurs in the polygon.

We transform $z(s)$ to discrete data $z[i]$, which is expressed as follows:

$$z[i] = x[i] + jy[i] \tag{11}$$

where i is seen as a natural number.

The Fourier coefficient $C_g[k]$ could be obtained by applying the discrete Fourier transform (DFT) of Formula (12) to $z[i]$. In it, N is the discrete data number, and k is in the range $0 \leq k \leq N-1$. According to this, it was possible to obtain N Fourier coefficients.

$$C_g[k] = \frac{1}{N}\sum_{i=0}^{N-1} z[i]\exp(-j\frac{2\pi}{N}ki) \tag{12}$$

Here, if the IDFT without low-pass filtering was applied to the obtained Fourier coefficient, it was possible to obtain the coordinate $z[i]$ of the original curve. The expression of the mathematics of the IDFT principles is expressed as follows:

$$z[i] = \sum_{k=0}^{N-1} C_g[k]\exp(j\frac{2\pi}{N}ki) \tag{13}$$

The IDFT that applied low-pass filtering was considered, and low-pass filtering used only the low-frequency component of the data number N. Because low domain composition ranges were dissimilar according to the kc value, on the basis of kc, the results after applying the Fourier descriptor became dissimilar. The range of low domain components was $0 \leq k \leq kc$ and $N - kc \leq k \leq n - N - 1$. The coordinate $z[i]$ could be obtained by low-pass filtering the Fourier coefficient $C_g[k]$ and performing the IDFT.

Applying a low-pass filtered IDFT is expressed as follows:

$$\tilde{z}[i] = C_g[0] + \sum_{k=1}^{kc} \begin{matrix}\{C_g[k]\exp(j\frac{2\pi}{N}ki) \\ +C_g[N-k]\exp(-j\frac{2\pi}{N}ki)\}\end{matrix} \tag{14}$$

This was obtained by converting Formula (13) of the IDFT into the form of low-pass filtering.

In the places where the Fourier descriptor should be applied, it should be separated based on vehicle areas that should be defined. In order to prevent problems that cannot be separated due to the shape of the different regions in the conventional method, the shape of the area was adjusted and the place to be separated was clarified. To do so, the G-shaped Fourier descriptor was used, and certain parameters were used for the G type Fourier descriptor. The details are as follows.

N : coordinate number of the histogram's outline.

$z[i]$: the coordinate of the outline's pixel.

i natural number of $0 \leq i \leq N-1$, and it is the coordinate of the pixel.

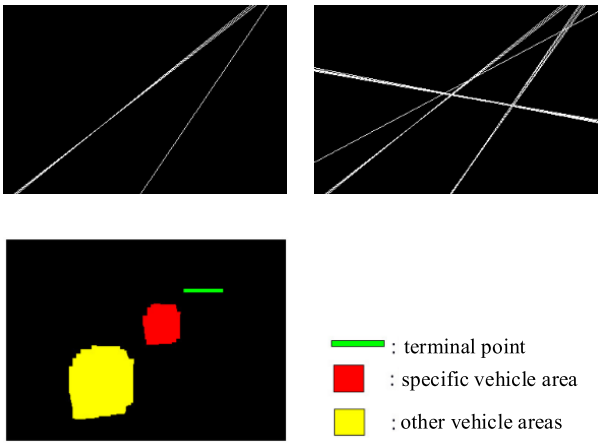

FIGURE 7. Gravity center extraction of the vehicle area based on the extracted road lines.

In order to assume a straight line in the direction of travel of the traveling vehicle, the proposed method used the white line on the road and the vehicle area center. For making the width of the extracted edges the same, the Hilditch thinning algorithm was applied to the extracted edge image. Through this process, the pixel width of the edge could be assigned a value. In order to make the extracted edge widths the same, the Hilditch algorithm was applied to extract the edge picture using the Laplacian filter. On the basis of this process, it was possible to make an edge of one pixel.

The method of pixel coordinates in the vehicle area could find the gravity of the vehicle area. A specific vehicle area was tracked from the vehicle area that passed through the installed window. The specific vehicle area was the number of vehicles passing through the window. Therefore, one center of gravity in each frame from the specific vehicle area could be obtained. It was possible to obtain the center of gravity (x, y) on the basis calculation as follows:

$$\begin{aligned} y &= \frac{1}{K}\sum_{i=1}^{K} y_i \\ x &= \frac{1}{K}\sum_{i=1}^{K} x_i \end{aligned} \tag{15}$$

Here, K is the amount of the specific vehicle area's connected pixel, and i is the pixel coordinate.

When a specific vehicle area reaches the end point, the center of gravity for multiple frames was plotted. The plot of the center of gravity is shown in Figure 8. By applying the Hough transformation to the plotted center of gravity, it was possible to extract a straight line as shown in Figure 9.

The angle θ of the straight line from the extracted straight line should be found. Therefore, from Figure 10, the following parameters concerning the straight line were detected. The relevant parameters of the line were as follows.

$(x1, y1)$: intersection of the straight line and the x axis at $y = 1$

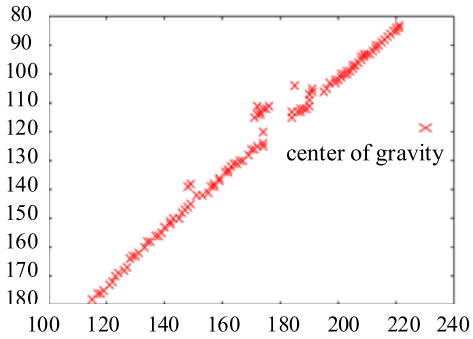

FIGURE 8. Plotting of gravity.

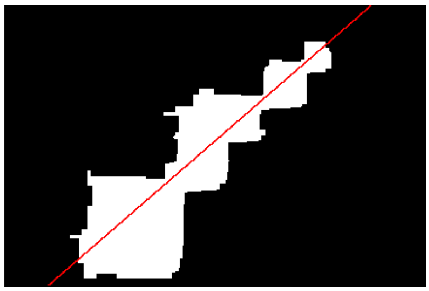

FIGURE 9. Example of a line drawn from the center of gravity.

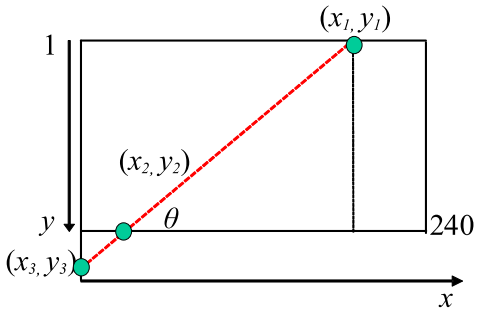

FIGURE 10. Linear Parameter Diagram.

$(x2, y2)$: intersection of the straight line and the x axis at $y = 240$.

$(x3, y3)$: intersection of the straight line and the y axis

By using Formula (16), it was possible to obtain the angle θ of the straight line.

$$\theta = \arctan\left(\frac{y2 - y1}{x1 - x2}\right) \times \frac{180}{\pi} \tag{16}$$

From the value, it was possible to extract a straight line with a small angular difference if the camera was fixed. Therefore, a straight line in the traveling direction of the traveling vehicle was extracted using the center of gravity of the vehicle area. Affine transformation formulas that are processed by parallel motion and rotation are used. The affine transformation of the vehicle area was needed to use the extracted line as a pivot. The parameter used in the affine transformation was the parameter of the detected straight line in Figure 10. The affine transform was applied to the vehicle area, and it needed to use the area to construct the histogram of the vehicle area.

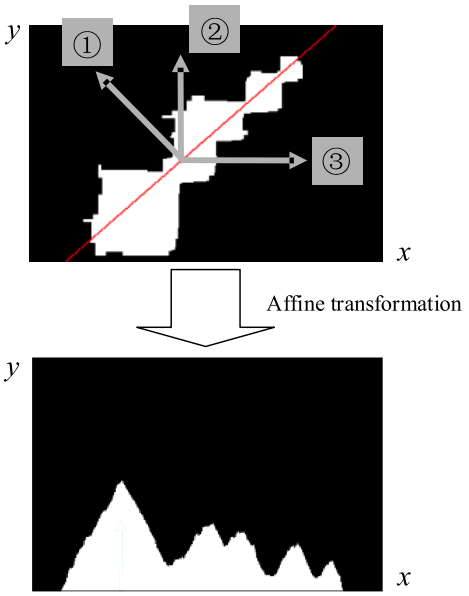

FIGURE 11. Histogram projection method for the vehicle area.

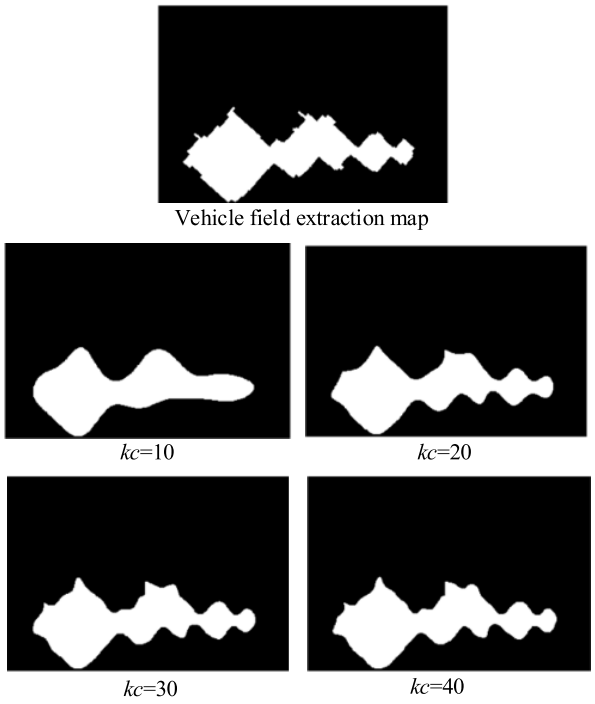

FIGURE 12. Fourier descriptor applied to the vehicle area.

In addition, it was necessary to put the affine transformed vehicle area into the picture. The projection was made perpendicular to the x axis with respect to the vehicle area to which the affine transformation was applied.

Figure 11 shows the three histogram projection methods. The projection of this study calculates the number of pixel values of 1 that are part of a vehicle area in one direction from a straight line pixel.

In order to solve the problem in which the shapes of the different regions in the conventional method could not be

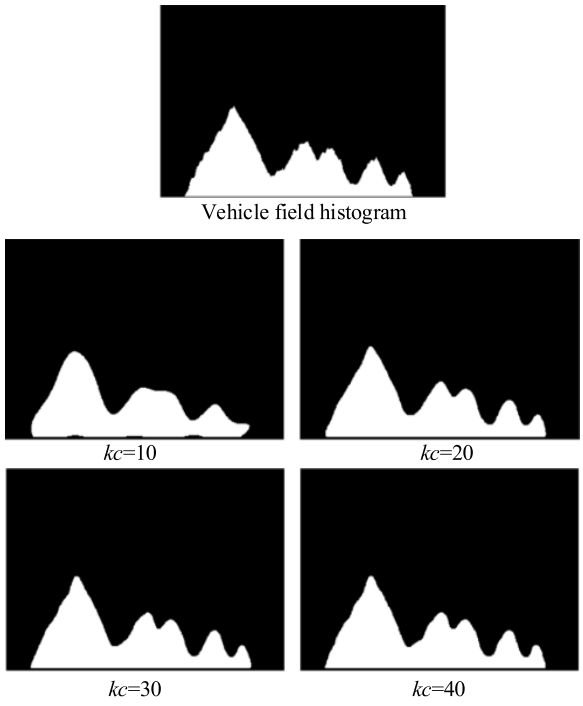

FIGURE 13. Using the *G*-shaped Fourier descriptors to solve the vehicle overlap.

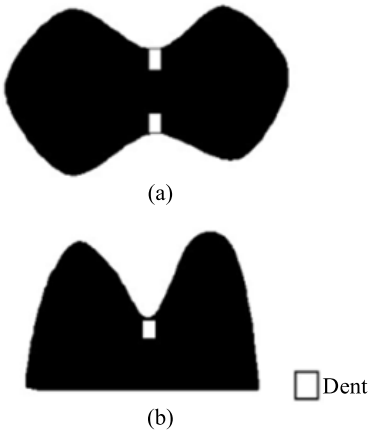

FIGURE 14. Overlap of vehicles. (a) Vehicle field. (b) Vehicle field histogram.

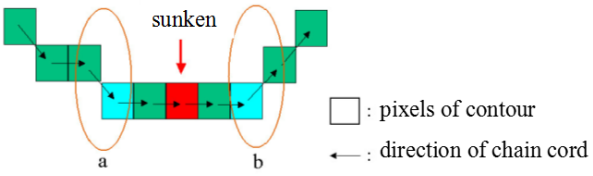

FIGURE 15. Detection of the indentations above the vehicle area.

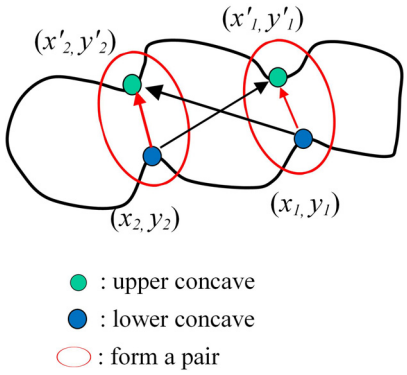

FIGURE 16. Drawing of dents in the vehicle area.

separated, the shape of the region needed to be adjusted, and the place to be separated needed to be removed. Therefore, we used the *G*-shaped Fourier descriptors to solve the problem of the precise segmentation of vehicle overlap. The applied results are shown in Figures 12 and 13. The applied results toward the vehicle area and histogram were dissimilar according to the low-pass filtering threshold *kc*. It was possible to arrange the vehicle shape areas by using the Fourier descriptor.

The vehicle regions based on the Fourier descriptors and the positions to be separated were detected through the histogram. The alternates of the places that should be separated were the sunken parts from the vehicle areas and histograms. These sunken parts are the square parts in Figure 14.

Figure 15 depicts a method for detecting dents from a vehicle area and a histogram. In order to detect dents in the vehicle area, the outline was extracted using a chain code. Two patterns were detected from the numerical sequence of the contour lines. Then, 4 or 0 intermediate indented pixels appear consecutively.

Figure 16 shows the drawing of the dents in the vehicle area. The coordinates of the upside sunken part pixel are (x'_j, y'_j), and the coordinates of the downside sunken part pixel are (x_i, y_i). i and j are the respective numbers. The distance d_{ij} between the upside sunken part and the downside sunken part could be obtained by using

$$d_{ij} = \sqrt{(x'_j - x_i) + (y'_j - y_i)} \tag{17}$$

i and j were combined, and j is the shortest distance from the upper recess i. For example, in Figure 15, (x_1, y_1) and (x'_1, y'_1) as well as (x_2, y_2) and (x'_2, y'_2) are groups.

In Figure 17, the upper part is the vehicle area, and the lower part is the histogram. The coordinate x of the vehicle area's sunken part is x'_j, and the sunken part coordinate x is x_k. The distance d'_{ik} between the histogram's sunken part and the vehicle area's sunken part could be obtained by

$$d'_{ik} = \left| x'_j - x_k \right| \tag{18}$$

where jk is the indentation of the jth vehicle area and the indentation of the kth histogram. d'_{ik} is a combination of the vehicle area j with the shortest distance from the histogram k.

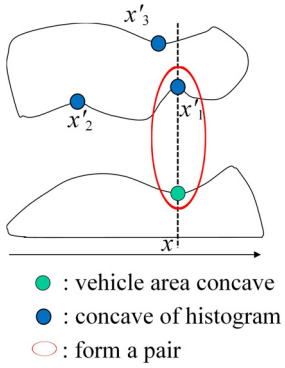

FIGURE 17. Drawing of the histogram and the sunken parts in the vehicle area.

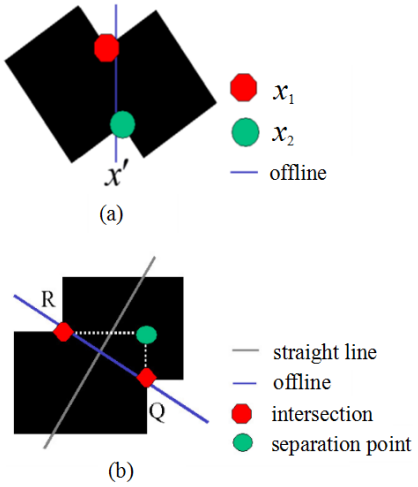

FIGURE 18. Detection points for area separation.

The separation position is performed by using the x-coordinate in the depression of the vehicle area that satisfies the separation condition.

Figure 18(a) is the vehicle area. The x-coordinate of the upper indentation is x_1, and the x-coordinate of the lower indentation is x_2. At this time, the separation position is set as the average value x' of the x coordinate. As shown in Figure 18(b), the intersection of the divider line and the vehicle area is R and Q. The line segment area connecting the separation point P and the point Q in the downward direction was replaced with the pixel value 0. Furthermore, the line segment area connecting the separation point and point R is replaced with a pixel value of 0. In this way, the overlapping position of the vehicle was separated.

IV. VEHICLE AREA SEPARATION EXPERIMENT BASED ON INTERNET OF THINGS MONITORING

The inter-frame difference method was used to extract the vehicle area from the image sequence. The entire vehicle area was formed from the contour image of the vehicle, which was obtained from the inter-frame difference image. Since unnecessary areas such as the shadows of the vehicle were also extracted, the unnecessary portions were deleted.

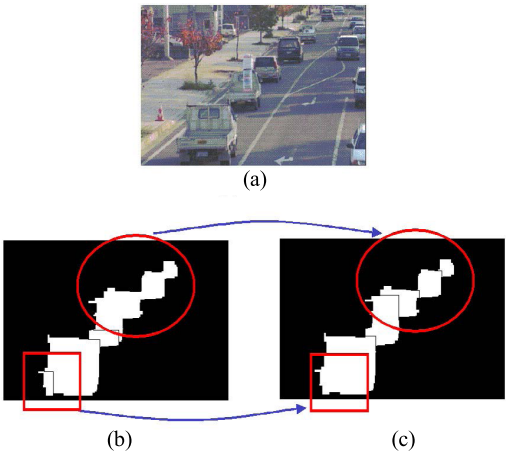

FIGURE 19. Vehicle area separation results based on the traditional method and the proposed method. (a) original image. (b) vehicle separation based on conventional method. (c) vehicle separation based on proposal method($kc = 30$).

TABLE 1. Accuracy verification judgment conditions.

Condition	Judgement Content	Judgement result
Condition 1	separated in the places that should be separated	success
Condition 2	separated in the places that should not be separated	failure
Condition 3	not separated in the places that should be separated	failure

In addition, the Fourier descriptor was used to separate the vehicle area before tracking the vehicle.

Figure 19 shows the result of applying the proposed method for monitoring video data based on the Internet of Things. Figure 19(a) is the original image with the overlapping vehicles that could not be separated using the conventional method (Figure 19(b)). Figure 19(c) is the vehicle separation result with the G type Fourier descriptor where $kc = 30$. The overlapping vehicles could be separated by the proposed method.

In order to determine the validity of the proposed method, the following method was used to verify the success rate. Initially, 100 frames were arbitrarily selected from the output image that executed the processing. Next, separation states were classified into three types of conditions, which are shown in Table 1. Condition 1 was a success, and 2 or 3 were failures.

Formula (19) was used to compute the success rate S from the measured result, where C is the number of measured results that meet the three types of conditions.

$$S = \frac{|C_1|}{C_1 + C_2 + C_3} \tag{19}$$

Table 2 shows the success rate of the proposed method, and Figure 19 is the expression of Table 2 in a graph. The threshold kc in Table 2 and Figure 19 is the threshold kc for low-pass filtering in the Fourier descriptor. In addition, when kc=0, the success rate was obtained by the previous method.

TABLE 2. Success rate of vehicle separation.

Threshold *kc*	C_1	C_2	C_3	S (%)
10	130	69	95	44.2
20	185	81	32	62.1
30	198	90	24	63.5
40	215	79	25	67.4
50	204	88	19	65.6
60	198	90	19	64.5
80	190	100	19	61.5
100	196	87	19	64.9

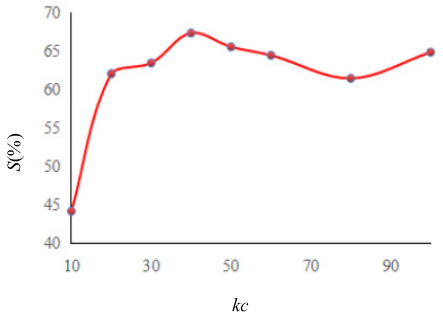

FIGURE 20. The relationship between separation success rate and *kc*.

Through the analysis of Table 2 and Figure 20, the following could be obtained.

When kc=10, the success rate was 44.2% and the success rate increases along with an increase in kc.

After $kc = 40$, the success rate's change decreases. There was no big change in the number of C_3, but the number of C_2 increases.

The reason for this result could be that the G type Fourier descriptor was processed using low-pass filtering. The low frequency component with respect to the data number N of the vehicle area contour line was $0 \leq k \leq kc$, $N - kc \leq k \leq N - 1$. When the number of vehicles with overlapping vehicles was small, the value of N decreased. Conversely, when the number of vehicles was large, the value of N became larger. The Fourier descriptor was applied to the extraction of the vehicle area, and a straight line was extracted based on the center of gravity of the vehicle area. The angles of lines with and without Fourier descriptors applied to the vehicle area are shown in Table 3.

Figure 21 shows the data in Table 3. It could be seen that when $kc = 0$, three of the four dispersion values became smaller. The reason for this result was that by applying the Fourier descriptor to the vehicle area, it could be considered that the shape of the area had been adjusted, and the correlation of the center of gravity had been increased to some extent. Finally, the angle averages and variances of the five data in Table 3 were 42.6 and 0.08.

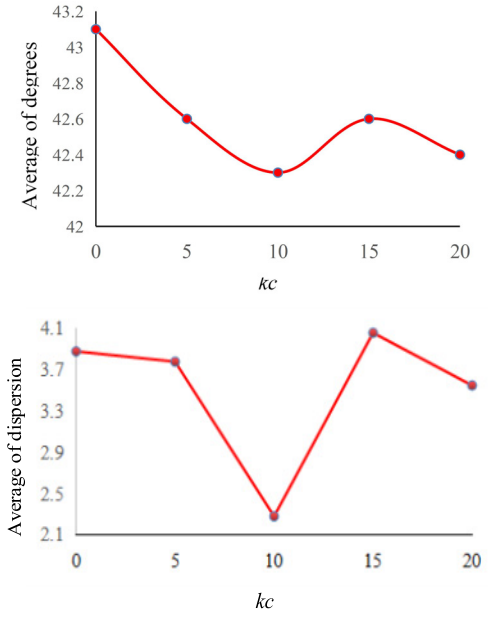

FIGURE 21. Average and dispersion graphs in Table 3.

TABLE 3. Results of the straight line angle θ when Fourier descriptors were applied.

kc	Average (degrees)	Variance (degrees)
0	43.1	3.88
5	42.6	3.78
10	42.3	2.28
15	42.6	4.06
20	42.4	3.55

V. DISCUSSION AND CONCLUSION

In this research, we proposed a method based on the Fourier descriptor to improve separation accuracy of vehicles in the Internet of Things surveillance video. It is a method of separating the area from the place to be separated, even if overlapping vehicles could not be separated by the conventional method. The proposed method can solve the problem of detection and segmentation of overlapping vehicles in an Internet of Things traffic video scene, and it can reduce the errors in vehicle detection and tracking.

It has been demonstrated through argumentation and experimentation that it is important to select the appropriate *kc* for each vehicle number in which the vehicle area overlaps for the separation of the vehicle. Specifically, the location is prepared by using the Fourier descriptor. The experimental results showed that the proposed method could accurately segment the majority of overlapping vehicles. In future research, it is necessary to detect how many vehicles overlap in the vehicle area and select an appropriate kc according to the number of vehicles. In order to measure the improvement of separability, the correlation between vehicle field separation and vehicle tracking accuracy should also be studied in future research.

REFERENCES

[1] S. Djahel, R. Doolan, G.-M. Muntean, and J. Murphy, "A communications-oriented perspective on traffic management systems for smart cities: Challenges and innovative approaches," *IEEE Commun. Surveys Tuts.*, vol. 17, no. 1, pp. 125–151, Mar. 2015.

[2] J. A. Guerrero-Ibanez, S. Zeadally, and J. Contreras-Castillo, "Integration challenges of intelligent transportation systems with connected vehicle, cloud computing, and Internet of Things technologies," *IEEE Wireless Commun.*, vol. 22, no. 6, pp. 122–128, Dec. 2015.

[3] K. Cui and X. Qin, "Virtual reality research of the dynamic characteristics of soft soil under metro vibration loads based on BP neural networks," *Neural Comput. Appl.*, vol. 29, no. 5, pp. 1233–1242, 2018.

[4] A. Arora *et al.*, "A line in the sand: A wireless sensor network for target detection, classification, and tracking," *Comput. Netw.*, vol. 46, no. 5, pp. 605–634, Dec. 2004.

[5] M. Balfaqih, M. Ismail, R. Nordin, A. A. Rahem, and Z. Balfaqih, "Fast handover solution for network-based distributed mobility management in intelligent transportation systems," *Telecommun. Syst.*, vol. 64, no. 2, pp. 325–346, 2017.

[6] L. Zhuo, L. Jiang, Z. Zhu, J. Li, J. Zhang, and H. Long, "Vehicle classification for large-scale traffic surveillance videos using convolutional neural networks," *Mach. Vis. Appl.*, vol. 28, no. 7, pp. 793–802, 2017.

[7] Y. Chen, G. Tao, H. Ren, X. Lin, and L. Zhang, "Accurate seat belt detection in road surveillance images based on CNN and SVM," *Neurocomputing*, vol. 274, pp. 80–87, Jan. 2018.

[8] J. Ren, C. Zhang, L. Zhang, N. Wang, and Y. Feng, "Automatic measurement of traffic state parameters based on computer vision for intelligent transportation surveillance," *Int. J. Pattern Recognit. Artif. Intell.*, vol. 32, no. 4, p. 1855003, 2018.

[9] D. Liu, Z. Lu, T. Cao, and T. Li, "A real-time posture monitoring method for rail vehicle bodies based on machine vision," *Vehicle Syst. Dyn.*, vol. 55, no. 6, pp. 853–874, 2017.

[10] L. Yang, B. Wang, R. Zhang, H. Zhou, and R. Wang, "Analysis on location accuracy for the binocular stereo vision system," *IEEE Photon. J.*, vol. 10, no. 1, Feb. 2018, Art. no. 7800316.

[11] I. Giannoukos, C.-N. Anagnostopoulos, V. Loumos, and E. Kayafas, "Operator context scanning to support high segmentation rates for real time license plate recognition," *Pattern Recognit.*, vol. 43, no. 11, pp. 3866–3878, Nov. 2010.

[12] D. Calabuig, D. Martín-Sacristán, J. F. Monserrat, M. Botsov, and D. Gozálvez, "Distribution of road hazard warning messages to distant vehicles in intelligent transport systems," *IEEE Trans. Intell. Transp. Syst.*, vol. 19, no. 4, pp. 1152–1165, Apr. 2018.

[13] S. Zhu, M. Gu, and J. Liu, "Moving vehicle detection and tracking algorithm in traffic video," *Indonesian J. Elect. Eng. Comput. Sci.*, vol. 11, no. 6, pp. 3053–3059, 2013.

[14] M. Swathy, P. S. Nirmala, and P. C. Geethu, "Survey on vehicle detection and tracking techniques in video surveillance," *Int. J. Comput. Appl.*, vol. 160, no. 7, pp. 22–25, 2017.

[15] A. Jazayeri, H. Cai, J. Y. Zheng, and M. Tuceryan, "Vehicle detection and tracking in car video based on motion model," *IEEE Trans. Intell. Transp. Syst.*, vol. 12, no. 2, pp. 583–595, Jun. 2011.

[16] J. Peng and Y. Shao, "Intelligent method for identifying driving risk based on V2V multisource big data," *Complexity*, vol. 2018, Apr. 2018, Art. no. 1801273.

[17] S. Noh, D. Shim, and M. Jeon, "Adaptive sliding-window strategy for vehicle detection in highway environments," *IEEE Trans. Intell. Transp. Syst.*, vol. 17, no. 2, pp. 323–335, Feb. 2016.

[18] W. Chu, Y. Liu, C. Shen, D. Cai, and X.-S. Hua, "Multi-task vehicle detection with region-of-interest voting," *IEEE Trans. Image Process.*, vol. 27, no. 1, pp. 432–441, Jan. 2018.

[19] J. L. Buliali, C. Fatichah, D. Herumurti, D. Fenomena, H. Widyastuti, and M. Wallace, "Vehicle detection on images from satellite using oriented fast and rotated brief," *J. Eng. Appl. Sci.*, vol. 12, no. 17, pp. 4500–4503, 2017.

[20] C. Mu, Z. Ni, C. Sun, and H. He, "Air-breathing hypersonic vehicle tracking control based on adaptive dynamic programming," *IEEE Trans. Neural Netw. Learn. Syst.*, vol. 28, no. 3, pp. 584–598, 2017.

[21] X. Wen, L. Shao, W. Fang, and Y. Xue, "Efficient feature selection and classification for vehicle detection," *IEEE Trans. Circuits Syst. Video Technol.*, vol. 25, no. 3, pp. 508–517, Mar. 2015.

[22] S. Sivaraman and M. M. Trivedi, "Active learning for on-road vehicle detection: A comparative study," *Mach. Vis. Appl.*, vol. 25, no. 3, pp. 599–611, 2014.

[23] Y. Tang, C. Zhang, R. Gu, P. Li, and B. Yang, "Vehicle detection and recognition for intelligent traffic surveillance system," *Multimedia Tools Appl.*, vol. 76, no. 4, pp. 5817–5832, 2017.

[24] X. Zhang, H. Gao, C. Xue, J. Zhao, and Y. Liu, "Real-time vehicle detection and tracking using improved histogram of gradient features and Kalman filters," *Int. J. Adv. Robot. Syst.*, vol. 15, no. 1, p. 1729881417749949, 2018.

[25] H. Kim, B. Liu, C. Y. Goh, S. Lee, and H. Myung, "Robust vehicle localization using entropy-weighted particle filter-based data fusion of vertical and road intensity information for a large scale urban area," *IEEE Robot. Autom. Lett.*, vol. 2, no. 3, pp. 1518–1524, Jul. 2017.

[26] Y. Cai, H. Wang, X. Chen, L. Gao, and L. Chen, "Vehicle detection based on visual saliency and deep sparse convolution hierarchical model," *Chin. J. Mech. Eng.*, vol. 29, no. 4, pp. 765–772, 2016.

[27] X. Yuan, S. Su, and H. Chen, "A graph-based vehicle proposal location and detection algorithm," *IEEE Trans. Intell. Transp. Syst.*, vol. 18, no. 12, pp. 3282–3289, Dec. 2017.

[28] M. S. Kim, Z. Liu, and D. J. Kang, "On road vehicle detection by learning hard samples and filtering false alarms from shadow features," *J. Mech. Sci. Technol.*, vol. 30, no. 6, pp. 2783–2791, 2016.

[29] H. Zhu, H. Fan, F. Ye, S. Zhu, and P. Gan, "A novel method for moving vehicle tracking based on horizontal edge identification and local autocorrelation images," *DYNA-Ingeniería e Ind.*, vol. 91, no. 1, pp. 61–68, 2016.

[30] E. Corman, J. Solomon, M. Ben-Chen, L. Guibas, and M. Ovsjanikov, "Functional characterization of intrinsic and extrinsic geometry," *ACM Trans. Graph.*, vol. 36, no. 2, p. 14, 2017.

[31] C. Bi, Y. Yuan, R. Zhang, Y. Xiang, Y. Wang, and J. Zhang, "A dynamic mode decomposition based edge detection method for art images," *IEEE Photon. J.*, vol. 9, no. 6, Dec. 2017, Art. no. 7803813.

[32] E. Sokic and S. Konjicija, "Phase preserving Fourier descriptor for shape-based image retrieval," *Signal Process., Image Commun.*, vol. 40, pp. 82–96, Jan. 2016.

HONGHUI FAN received the M.S. and Ph.D. degrees from the Faculty of Engineering, Yamgata University, Japan, in 2008 and 2011, respectively. He is currently an Associate Professor with the College of Computer Engineering, Jiangsu University of Technology. His research interests include computer application technology, image processing, and image restoration.

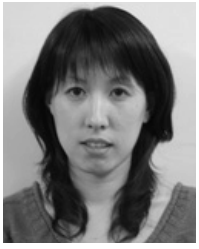

HONGJIN ZHU received the M.S. and Ph.D. degrees from the Faculty of Engineering, Yamgata University, Japan, in 2006 and 2010, respectively. She is currently an Associate Professor with the College of Computer Engineering, Jiangsu University of Technology. Her research interests include image processing, computer vision, and pattern recognition.